ARTICLE

Check for updates

Hedyotis diffusae Herba-*Andrographis* Herba inhibits the cellular proliferation of nasopharyngeal carcinoma and triggers DNA damage through activation of p53 and p21

Zhiqing Liu[1,4], Shan Mu[1,4], Sha Li[1], Jiao Liang[1], Yuanyuan Deng[2], Zuo Yang[1], Jiongke Li[1], Liu Cao[3], Qinwei Fu[1], Xiaodong Chen[1], Lingyan Ding[1], Rui Han[1], Qinxiu Zhang[1]✉ and Hui Xie[1]✉

Dysregulation of the cell cycle and the resulting aberrant cellular proliferation has been highlighted as a hallmark of cancer. Certain traditional Chinese medicines can inhibit cancer growth by inducing cell cycle arrest. In this study we explore the effect of *Hedyotis diffusae* Herba-*Andrographis* Herba on the cell cycle of nasopharyngeal carcinoma (NPC). *Hedyotis diffusae* Herba-*Andrographis* Herba-containing serum was prepared and then added to the cell culture medium. BrdU, comet, and FUCCI assays, western blot analysis and flow cytometry analysis revealed that *Hedyotis diffusae* Herba-*Andrographis* Herba treatment significantly alters cell proliferation, DNA damage, and cell cycle distribution. Xenograft mouse model experiments were performed, confirming these in vitro findings in vivo. Treatment with *Hedyotis diffusae* Herba-*Andrographis* Herba inhibited cell proliferation, promoted DNA damage, and arrested NPC cells progression from G1 to S phase. Further examination of the underlying molecular mechanisms revealed that treatment with *Hedyotis diffusae* Herba-*Andrographis* Herba increased the expression of p53 and p21, while reducing that of CCND1, Phospho-Rb, E2F1, γH2AX, and Ki-67 both in vivo and in vitro. Conversely, the inhibition of p53 and p21 could abolish the promoting effect of *Hedyotis diffusae* Herba-*Andrographis* Herba on the NPC cell cycle arrest at the G1 phase, contributing to the proliferation of NPC cells. *Hedyotis diffusae* Herba-*Andrographis* Herba suppressed the tumor growth in vivo. Overall, these findings suggest that *Hedyotis Diffusae* Herba-*Andrographis* prevent the progression of NPC by inducing NPC cell cycle arrest at the G1 phase through a p53/p21-dependent mechanism, providing a novel potential therapeutic treatment against NPC.

Cancer Gene Therapy (2022) 29:973–983; https://doi.org/10.1038/s41417-021-00385-7

INTRODUCTION

Nasopharyngeal carcinoma (NPC) is a common head and neck malignancy and has a distinct geographical and ethnic distribution [1], being especially common in Eastern and Southeastern Asia [2]. NPC is an epithelial malignant tumor that occurs on the upper surface of the pharyngeal mucosa, with most cases being accompanied by Epstein-Barr virus infections [3]. The development of NPC is mainly attributed to environmental, lifestyle choices, and genetic factors [4]. In recent years, the incidence and fatal cased of NPC have gradually decreased due to lifestyle changes, improved population screening, better radiotherapy treatments, as well as the effective application systemic drugs [5]. Despite this, NPC still accounts for 1% of cancer related deaths in China [6].

Traditional Chinese medicine has been used to treat a variety of cancers for a long time [7, 8]. For example, Liao YH, et al. have demonstrated that traditional Chinese medicine increases the survival of patients with liver cancer [9]. In addition, an earlier study has indicated that traditional Chinese medicine can reduce the risk of death in breast cancer patients [10]. Of note, traditional Chinese medicine is becoming recognized as an effective therapy for the treatment of NPC [11, 12]. *Hedyotis diffusae* Herba (Family Rubiaceae) and *Andrographis paniculata* (Family Acanthacea) Herba are two herbs commonly used in traditional Chinese medicine treatments. *Hedyotis diffusae* Herba exerts an inhibitory effect on hepatoma cancer, which may be related to the enhancement of the body's innate immune function, as well as cytotoxic effects [13]. *Hedyotis diffusae* Herba has been used to successfully treat advanced NPC patients, leading to a reduction in the overall and cancer-related mortality risk [14]. *Andrographis paniculata* is a type of herbaceous plant containing an abundance of bioactive molecules, which are known to exert large scale anti-inflammatory and anticancer responses [15]. Treatment with *Andrographis* can suppress proliferation and stimulate apoptosis of C666-1 cells by upregulating the LKB1/AMPK/mTOR signaling pathway [16].

Bufalin, a cardiotonic steroid and a key active ingredient of the Chinese medicine ChanSu, has been revealed to lead to DNA damage and cellular apoptosis in NPC [17]. Additionally, Mukonal, a plant-derived carbazole alkaloid that has been used in traditional

[1]Department of Otolaryngology, Hospital of Chengdu University of Traditional Chinese Medicine, Chengdu, P. R. China. [2]Department of Traditional Chinese Medicine, Hi-tech Zhonghe Community Health Service Center, Chengdu, P. R. China. [3]Department of Ophthalmology and Otorhinolaryngology, Sichuan Integrative Medicine Hospital, Chengdu, P. R. China. [4]These authors contributed equally: Zhiqing Liu, Shan Mu. ✉email: zhangqinxiu@cdutcm.edu.cn; xh123@cdutcm.edu.cn

Received: 7 January 2021 Revised: 8 August 2021 Accepted: 27 August 2021
Published online: 9 November 2021

Chinese medicine to treat several types of cancer, has been shown to suppress the proliferation of NPC cells [18]. Moreover, cinobufagin, an active ingredient in Venenum bufonis, a product of the secretions of *Bufo gargarizans*, is capable of inhibiting cell proliferation in several types of tumor cells, and blocks NPC progression by blocking cell cycle at the S phase and thereby inducing apoptosis [19]. Andrographolide increases the expression of cell cycle inhibitory protein p27 and reduces the expression of cell-cycle-dependent kinase 4 (CDK4), which plays an anticancer role through the blockade of cell cycle by inducing arrest at the G0/G1 transition [20]. Treatment of liver cells with andrographolide caused a significant increase in the expression of p53 [21], a tumor suppressor that mainly acts as a transcription factor, activity of which regularly leads to cell cycle arrest [22]. Activation of p53 contributes to inhibited NPC cells colony formation, proliferation, tumor growth, migration and invasion, and augmented cell cycle arrest, with a marked increase in cells at the G1 stage and decrease in cells at S stage [23, 24]. The cyclin-dependent kinase inhibitor p21, a main effector of p53, modulates a variety of cellular functions including cell cycle progression and mediates cell cycle block in G1 phase in response to many stimuli such as oncogene-induced proliferation [25]. Activation of p21 has been reported to participate in G1 phase arrest in NPC cells [26]. Nuclear DNA damage has been shown to induce the activation of p53, which drives p21 activation to mediate the expression of cyclin-dependent kinases 4 and 6 (CDK4/6) and cyclin D1 (CCND1) [27]. As a response to growth factor stimulation or oncogenic signals, CCND1 activates CDK4/6, promoting the transition from G1 to S cell cycle by phosphorylation and inactivation of tumor suppressor retinoblastoma (Rb) protein. The inactivated Rb is then released from a complex with transcription factor E2F transcription factor 1 (E2F1), which can then freely initiate DNA replication and the expression of mitosis-related genes, thereby inducing cell proliferation [28].

Based on these findings, we hypothesized that the combination of *Hedyotis diffusae* Herba and *Andrographis* Herba may interfere with NPC progression through regulation of DNA damage, cell proliferation, and cell cycle arrest by modulating p53, p21, and CCND1 expression. In this study we test this hypothesis, showing that *Hedyotis diffusae* Herba-*Andrographis* Herba affects NPC progression through regulation of the p53/p21/CCND1 regulatory axis, identifying a molecular mechanism which could be used as a potential therapeutic target for the treatment of NPC.

MATERIALS AND METHODS

Preparation of drug-containing serum

Hedyotis diffusae Herba-*Andrographis* Herba (30 g) and *Andrographis paniculata* (15 g) were purchased from Bozhou Baichuan Pharmaceutical Co., Ltd. (Guangdong, China). These medicinal materials were resuspended in water, decocted for 45 min and 30 min, and then concentrated by evaporation to 167 mL, meaning that every 1 mL of medicinal solution contained 0.27 g of Chinese medicine [29]. Concentrated drugs were stored at 4 °C. Twelve male specific pathogen-free (SPF) Sprague-Dawley (SD) rats (weighing 190–230 g; 101, Vital River Laboratory Animal Technology Co., Ltd., Beijing, China) were assigned into a *Hedyotis diffusae* Herba-*Andrographis* Herba group and a Vehicle group, with six rats in each group. The dose given to rats (D3) was: D3 = D1 × 6.25 mg/kg (where D1 is the human dose). The adult dose of 45 g/60 kg/day thus converts to the rat dose: D3 = 45 g ÷ 60 kg × 6.25 × 0.2 kg = 0. 938 g/day. Each rat in the *Hedyotis diffusae* Herba-*Andrographis* Herba group received intragastric administration twice a day with (0. 938 g/day ÷ 2 times ÷ 0.27 g/mL) 1.7 mL of the concentrated medicine [29]. Six rats in the *Hedyotis diffusae* Herba-*Andrographis* Herba group were subjected to intragastric administration with 1.7 mL of *Hedyotis diffusae* Herba-*Andrographis* Herba twice daily for 7 days and six rats in the Vehicle group were subjected to intragastric administration with equal volume of normal saline twice daily for 7 days. Two hours after the last intragastric administration, 0.3% amobarbital sodium was intraperitoneally injected into the abdominal cavity of rats for anesthesia. Blood was collected from the abdominal aorta under sterile conditions. Serum was removed and inactivated at 56 °C for 30 min, followed by filtration through a 0.22 μm filter membrane for sterilization. The drug-containing serum was prepared, mixed, and stored at −20 °C.

Cell culture and transfection

Human NPC cell lines C666-1 (CC-Y1082) and SUNE-1 (CC-Y1486) were purchased from Shanghai Biological Technology Co., Ltd., enzyme research (Shanghai, China) and cultured in Roswell Park Memorial Institute (RPMI) −1640 medium (CC-Y1082M, Shanghai Biological Technology Co., Ltd., enzyme research, Shanghai, China) supplemented with fetal bovine serum (FBS, Gibco) and 1% penicillin and streptomycin in an incubator at 37 °C containing 5% CO_2. The cells were then detached with 0.25% trypsin and passaged. The cells at the logarithmic growth phase were used for the experiment.

After the cells were cultured for 12 h, the medium was removed. Thereafter, drug-containing serum was added to the cell culture medium and blank serum to the control group, with 10 mL of the drug-containing serum supplemented to every 100 mL of cell culture medium. Recombinant human p53 adenovirus (rAd-p53)-transduced C666-1 and SUNE-1 cells were subsequently constructed. According to the manufacturer's instructions, the cells were transduced with rAd-p53 upon reaching 40% confluence. After 24 h, positive cells were screened. The cells were treated with blank control, blank serum, drug-containing serum, cultured with medicated, or drug-free medium for 24 h; cells were treated with Pifithrin-α (PFTα) (p53 inhibitor, 63208-82-2, Selleck Chemicals, Houston, TX, USA, S2929) or UC2288 (p21 inhibitor, 2.5 μM; ab146969, Abcam Inc., Cambridge, UK).

Transmission electron microscope (TEM)

Cells in the logarithmic growth phase were seeded into six-well plates and cultivated to a subconfluent state. Cells were incubated in medium containing normal serum or drug-containing serum or in serum-free medium for 24 h. The cells were collected and centrifugated twice in 0.1 mol/L phosphate buffer (pH 7.4). After being fixed with 2.5% glutaraldehyde for at least 2 h, cells were stained with 1% osmium tetroxide for 30 min, dehydrated with an acetone concentration series, and placed in Epon 812 resin at room temperature overnight. Ultra-thin sections were cut and mounted on a copper mesh, followed by staining with uranium acetate and lead citrate. The stained grid was examined and imaged under a transmission electron microscope (TEM; Hitachi, Tokyo, Japan).

Alkaline comet assay

Cells were collected and resuspended in chilled PBS. Trypan blue staining was used to determine cell viability. The number of trypan blue-positive cells did not exceed 15%. Two slides were prepared for each sample, with two gels being used for each slide. The sections were soaked and dissolving in solution supplemented with 2.5 M NaCl, 100 mM ethylenediamine tetraacetic acid (EDTA), 10 mM Tris, 0.16 M dimethyl sulfoxide, and 0.016 mM Triton X-100 for 1 h (with the final pH value adjusted to 10), and then washed three times with PBS (5 min per wash). Thereafter, each sample was treated with the mixture of formamide-pyrimidine-glycosylase (FPG) and endonuclease III (ENDO III) (i.e., two gels) at a ratio of 1:1. Each gel was exposed to 45 μL of enzyme mixture (the final concentration of both enzymes was 2.5 μg/mL; Sigma–Aldrich Chemical Company, St Louis, MO, USA) at 37 °C for 30 min. At the same time, the remaining gel of each sample was treated with the same volume of enzyme dilution buffer (0.1 M KCl, 4 mM EDTA, 2.5 mM 4-(2-hydroxyethyl)-1-piperazineëthanesulfonic acid [HEPES], and 2% bovine serum albumin [BSA]). The slides were equilibrated in alkaline buffer (0.3 M NaOH, 1 mM EDTA, pH 13) for 40 min to induce unfolding of the DNA, followed by electrophoresis in alkaline buffer for 30 min at 4 °C, 1 V/cm and 300 mA. Finally, the slides were neutralized with 0.4 M Tris (pH 7.5), stained with 0.005% ethidium bromide (Sigma–Aldrich) for 7 min, washed with distilled water for 7 min, fixed with methanol for 15 min, dried at room temperature, and stored at 4 °C.

Before analysis, the slides were rehydrated in distilled water, and the images were recorded with a CCD-13008 camera (VDS, Vosskuhler, Germany) and a BX51 fluorescence microscope (Olympus, Tokyo, Japan). The degree of DNA migration was quantified using Lucia Comet Assay 7.00 software (Laboratory Imaging, Prague, Czech Republic). The percentage of comet tail area (the proportion of the DNA tail area to the total DNA area) and the length of the comet tail (from the center of the DNA head to the end of the DNA tail) of 50 cells were subjected to monolithic analysis. The experiment was conducted three times independently [30].

Cell viability test

Cells in the logarithmic growth phase were seeded in six-well plates and cultured to a subconfluent state. Cells were incubated in medium containing blank serum (blank serum group), drug-containing serum alone (drug-containing serum group) or in presence of MDM2i (drug-containing serum + MDM2i group) or UC2288 (drug-containing serum + UC2288 group), or in serum-free medium (blank control group) for 24 h. Cell viability was determined using a Cell Titer-Blue Cell Viability Assay kit as per the manufactures protocol (G8080, Promega, Madison, WI, USA). Cells were fixed with 100% methanol for 10 min, followed by staining with 1% crystal violet solution (Sigma–Aldrich). The fluorescence value was measured with a 96-well plate fluorescence microplate reader (Thermo Scientific Varioskan LUX, Waltham, USA) and then observed and imaged under a microscope (Olympus). Cells cultured in the serum-free medium was considered to be 100% viable cells.

Immunofluorescence staining

Bromodeoxyuridine (BrdU) is a synthetic thymidine nucleotide analog, which can be incorporated into newly synthesized synthetic DNA in replicating cells (cell cycle S phase). C666-1 and SUNE-1 cells in the logarithmic growth phase were seeded in six-well plates at a density of 1×10^6 cells/well. The cells were treated with drug-containing or control medium along with 10 μg/mL BrdU (Sigma, St. Louis, MO, USA) for 30 min at room temperature. After the supernatant was medium, the cells were fixed with 4% paraformaldehyde for 10 min, pretreated with 2 M HCl for 20 min and permeabilized with 0.5% Triton X-100 for 10 min. The cells were then blocked with 10% goat serum for 1 h and probed with anti-BrdU monoclonal rat primary antibody (1: 300, Sigma, St. Louis, MO, USA) overnight. The following day, the cells were reprobed with goat anti-rabbit IgG (H&L, Alexa Fluor® 647, 1:1000, Abcam, ab150087), and treated with 4′-6-diamidino-2-phenylindole (DAPI) or nuclear staining. Images were photographed under a fluorescence microscope (Olympus) and the percentage of BrdU-positive cells was calculated.

Colony formation assay

C666-1 and SUNE-1 cells were seeded in six-well plates at a density of 5×10^2 cells/well. Cells were cultured in serum-free medium or drug-containing medium for 1 week (the cells formed visible clones). After the medium was removed, the cells were fixed with 4% paraformaldehyde (Shanghai Sangon, Shanghai, China) for 15 min. The cells were stained with crystal violet (Shanghai Sangon) for 30 min and then counted.

Fluorescence ubiquitination cell cycle indicator (FUCCI)

A NPC cell line expressing FUCCI was established in order to be able to examine cell cycle progression. Briefly, C666-1 and SUNE-1 cells were transfected with FUCCI-S/G2/M green vector (AM-V9010M; MBL Life Science). Next, 1 μg Lipofectamine 2000 (Thermo Fisher Scientific Inc., Waltham, MA, USA) and 500 mM antibody-free medium were used to transfect 500 ng plasmids into groups of 2×10^5 cells. On the 3rd day post transfection, the cells were treated with neomycin-containing medium for screening, and were then seeded and cloned by the limiting dilution technique. Community formed by stable cells was chosen, and FUCCI-G1 Orange vector (AM-V9003M; MBL Life Science) was transfected into NPC cells expressing FUCCI-S/G2/M, followed by another neomycin screening.

Western blot analysis

Total protein from tissues or cells was extracted using enhanced radioimmunoprecipitation assay (RIPA) lysis buffer (Boster Biological Technology Ltd., Wuhan, China) supplemented with protease inhibitor. Protein concentration was detected using a bicinchoninic acid (BCA) protein assay kit as per the manufacturer's instructions (Boster). Isolated proteins were separated by 10% sodium dodecyl sulfate-polyacrylamide gel electrophoresis (SDS-PAGE) and transferred onto polyvinylidene fluoride (PVDF) membranes. The membrane was then blocked with 5% BSA for 2 h and probed with diluted primary anti-rabbit antibodies to p53 (ab131442), p21 (ab109199), CCND1 (ab226977), CDK2 (ab32147), Phospho-Rb (ab47763), E2F1 (ab179445), γ-H2AX (ab11175), β-actin (ab227387), and Lamin B1 (ab229025) overnight at 4 °C. The following day, the membrane was reprobed with the secondary goat anti-rabbit antibody (ab205719, 1: 2000) labeled by horseradish peroxidase (HRP) for 1 h at room temperature. The above-mentioned antibodies were from Abcam. The immunocomplexes on the membrane were visualized using enhanced chemiluminescence (ECL; EMD Millipore, Billerica, MA, USA) for 1 h. A Tanon 5200 visualizer was applied for development and band intensities were quantified using Image J software. The relative protein expression was calculated with β-actin and Lamin B1 as the internal reference.

Flow cytometry

Cells were seeded in a 6-well plate at a density of 1.5×10^6 cells/well. The cells were trypsinized, neutralized by serum-containing medium, centrifuged at 2000 rpm for 5 min, resuspended in precooled PBS, and washed. The supernatant was removed, leaving ~50 μL. Next, the cells were resuspended in 1 mL PBS to form a single-cell suspension, and treated with 3 mL of precooled absolute ethanol to a final concentration of 75%, and left to stand at 4 °C overnight (18–24 h). The cells fixed overnight, rinsed twice with cooled PBS, centrifuged at 2000 rpm for 5 min, and added with 200 μL PBS (~400 μL). Afterwards, the cells were resuspended in 20 μL RNase (storage concentration of 25 mg/mL, PBS diluted to 1 mg/mL, working concentration of 50 μg/mL), and then added with 20 μL PI to a final concentration of 50 μg/mL (storage concentration of 25 mg/mL, PBS diluted to 1 mg/mL, working concentration of 10 μL). The cells were stained in the dark at 4 °C for 30 min and then analyzed by flow cytometry within 24 h.

Tumor xenografts in nude mice

Thirty-six SPF BALB/c nude mice (aged 6 weeks, weighing 14–18 g; 401, Vital River Laboratory Animal Technology Co., Ltd., Beijing, China) were acclimatized for one week in the SPF laboratory at 20–25 °C and relative humidity of 45–50% with a 12 h light/dark cycle, with free access to feed and water. C666-1 and SUNE-1 cells were prepared into cell suspension at a density of 5×10^7 cells/mL. Next, 0.2 mL of the cell suspension was injected subcutaneously into the right armpit of each mouse. When the tumor volume reached 100 mm^3, the mice were randomly divided into a control group (without any treatment), a Vehicle group (intragastric administration of 0.25 mL of equal volume of normal saline twice daily for 30 days), and a *Hedyotis diff*usae Herba-*Andrographis* Herba group (intragastric administration of 0.25 mL of *Hedyotis diff*usae Herba-*Andrographis* Herba twice daily for 30 days) ($n = 12$/group). The tumors were measured every 2 days with a Vernier caliper and tumor volume calculated using the formula: $V = a \times b^2/2$, where V is tumor volume, a is the tumor length and b is the width. We plotted the tumor weights by treatment group as a function of time. Two hours after the last intragastric administration, the mice were euthanized and the subcutaneous tumor was extracted, weighed and photographed. No blinding was required.

Cell cycle detection in tumor tissues

Nude mice in each group were administered for 30 days and at 2 h after the final administration, the mice were euthanized and the subcutaneous tumors were removed. The tumor tissues were fixed in 4% paraformaldehyde for 24 h, dehydrated with 30% sucrose for 48 h, and embedded at −25 °C for frozen sections at a thickness of 5 μm. After allowed to stand at room temperature for 30 min, the sections were fixed in ice acetone for 10 min, rinsed thrice with PBS (5 min per wash), dried and mounted. Finally, the cell cycle distribution in the tumor tissue sections was analyzed under a fluorescence microscope, (S/G2/M phases: green and G0/G1 phases: red) [31].

Immunohistochemistry

Paraffin sections were dewaxed, hydrated, and washed with PBS. Antigen retrieval was carried out in 10 mM citrate buffer (pH 6.0) in a microwave oven for 20 min. After blocking with 3% hydrogen peroxide (H_2O_2) for 10 min, the sections were incubated with 0.1% Triton X-100 in PBS for 20 min, immersed in 5% BSA for 20 min and probed with primary anti-BrdU antibody (1: 100; ab152095; Abcam) at 4 °C overnight. After washing with PBS, the sections were reprobed with HRP-conjugated polyclonal goat anti-rabbit immunoglobulin G (IgG) for 1 h and developed with the peroxidase substrate diaminobenzidine (DAB). All sections were counterstained with hematoxylin and imaged under a microscope (Olympus).

Pharmacological analysis of Chinese medicine

The active ingredients and corresponding targets of *Hedyotis diffusae* Herba-*Andrographis* Herba were retrieved using the TCMSP database (https://tcmspw.com/tcmsp.php). According to the active ingredients' oral bioavailability (OB) and drug-likeness (DL), ingredients were screened with the criteria set as OB ≥ 15%, DL ≥ 0.18. With "nasopharyngeal carcinoma"

set as the keyword, the GeneCards database (https://www.genecards.org/) was used to retrieve the NPC-related targets (published molecular therapeutic targets). The intersection of the screening results of TCMSP and GeneCards database was taken to determine the potential target of *Hedyotis diffusae* Herba-*Andrographis* Herba in the treatment of NPC. The jvenn online tool (http://jvenn.toulouse.inra.fr/app/example.html) was adopted to identify the common targets of *Hedyotis diffusae* Herba-*Andrographis* Herba and NPC-related targets. The interaction relationship of candidate genes was analyzed using the STRING database (https://string-db.org/; minimum required interaction score = 0.9), and Cytoscape 3.5.1 software was utilized to visualize the interaction relationship network. The built-in tool NetworkAnalyzer was employed to analyze the network, with the Degree value of the gene calculated. The R language "clusterProfiler" package (https://bioconductor.org/packages/release/bioc/html/clusterProfiler.html) was used to perform Kyoto Encyclopedia of Genes and Genomes (KEGG) and gene ontology (GO) enrichment analyses on candidate genes. The relationship between pathway factors was identified by the KEGG database (https://www.genome.jp/kegg/pathway.html).

Statistical analysis

The data were processed using SPSS 21.0 statistical software (IBM Corp. Armonk, NY, USA). Measurement data were summarized by mean ± standard deviation throughout this study. Data obeying normal distribution and homogeneity of variance among multiple groups were compared using one-way analysis of variance (ANOVA) with Tukey's post-hoc test. Repeated measures ANOVA with Bonferroni post-hoc test was applied for the comparison of data among multiple groups at different timepoints. A value of $p < 0.05$ indicated significant difference.

RESULTS

Hedyotis diffusae Herba-*Andrographis* Herba inhibits the proliferation of NPC cells

Initially, the serum was isolated from rats treated with *Hedyotis diffusae* or Herba-*Andrographis* Herba, which was then added to NPC cell lines C666-1 and SUNE-1. A BrdU assay was performed in these NPC cells to determine if treatment effects the proliferation of C666-1 (Fig. 1A, B) and SUNE-1 (Fig. 1C, D) cells. The results showed that, when compared with cells treated with control blank serum, BrdU expression was significantly reduced in cells treated with drug-containing serum. This suggests that the *Hedyotis diffusae* Herba-*Andrographis* Herba treatment does in fact suppress the proliferation of NPC cells.

Hedyotis diffusae Herba-*Andrographis* Herba treatment inhibits the tumorigenicity of NPC in vivo

To determine the effects of *Hedyotis diffusae* Herba-*Andrographis* Herba on the tumorigenicity of NPC cells in vivo, we constructed a nude mouse xenograft model. Compared to mice receiving intragastric administration with saline, the tumor volume of mice receiving intragastric administration with *Hedyotis diffusae* Herba-*Andrographis* Herba was strikingly reduced (Fig. 2A, B). Meanwhile, similar results were obtained in the tumor weight of mice (Fig. 2C). Relative to mice receiving intragastric administration with normal saline, it was markedly reduced by the medical treatment (Fig. 2D). As shown in Fig. 2E, F, there was no significant difference in body weight of C666-1- and SUNE-1-implanted mice following administration. Importantly, intragastric administration of saline did not affect tumor volume or expression of BrdU in the tumor tissue when compared to untreated mice. Therefore, these results showed that as well as inhibiting NPC proliferation in vitro. *Hedyotis diffusae* Herba-*Andrographis* Herba inhibits tumorigenicity of NPC in vivo.

Hedyotis diffusae Herba-*Andrographis* Herba promotes DNA damage in NPC cells

OB and DL analysis on the active ingredients and corresponding targets of *Hedyotis diffusae* Herba-*Andrographis* Herba obtained from the TCMSP database revealed 33 active ingredients and 200 targets (Supplementary Table 1). In addition, 1857 published molecular therapeutic targets for NPC were identified using the GeneCards database. Following Venn diagram analysis of the predicted medication targets and therapeutic targets for NPC, 112 candidate targets were found in both data sets (Fig. 3A). Next, we plotted the intersection network of candidate targets and the active ingredients of *Hedyotis diffusae* Herba-*Andrographis* Herba plotted (Fig. 3B). Through the enrichment analysis of candidate genes, the KEGG signaling pathway, biological process (BP), molecular function (MF), and cellular component (CC) that the genes participated in were obtained (Fig. 3C-F). This enrichment analysis indicates that treatments which alleviate the NPC progression mainly act by regulating the proliferation, apoptosis, and DNA damage of NPC cells.

Moreover, the results of a comet assay displayed no significant difference in the percentage of TA to WA of DNA and the average comet tail length between cells without any treatment and those treated with the blank serum. The percentage in C666-1 cells treated with drug-containing serum was 31.08%, and the average comet tail length was 45.22 ± 3.36 μm ($p < 0.05$) while the percentage in SUNE-1 treated with drug-containing serum was 28.92%, and the average comet tail length was 36.59 ± 4.12 μm. In comparison to blank serum, the percentage of TA to WA and the average comet tail length were increased in C666-1 and SUNE-1 cells treated with drug-containing serum (Fig. 3G-I). These results appear to indicate that *Hedyotis diffusae* Herba-*Andrographis* Herba could potentially increase DNA damage in NPC cells as well as inhibiting DNA damage repair.

In order to explore these findings further we examined nontreated and treated C666-1 and SUNE-1 cells using TEM analysis. In contrast to untreated cells which displayed awell-preserved plasma membrane, the NPC cells treated with drug-containing serum had a distinctive altered morphology, with a small number of microvilli seen on the cell surface, and chromatin accumulation, indicating that these cells were in the early stages of apoptosis (Fig. 3J). Additionally, western blot analysis suggested no significant difference in the protein expression of γH2AX between untreated cells and those treated with blank serum. However, protein expression of γH2AX was markedly increased in cells treated with drug-containing serum compared with the cells treated with blank serum (Fig. 3K, L). Collectively, *Hedyotis diffusae* Herba-*Andrographis Herba* promoted DNA damage of NPC cells.

Hedyotis diffusae Herba-*Andrographis* Herba treatment blocks cell cycle of NPC cells

In order to examine cell cycle distribution more closely we adopted a FUCCI approach using C666-1 and SUNE-1 cells at 0, 3, 6, 9, 12, 15, 18, 21, and 24 h after treatment with *Hedyotis diffusae* Herba-*Andrographis Herba*. Following administration, an increase in cells arrested at the G0/G1 phase was detected, while as time passed fewer cells were observed to be arrested at the S/G2/M phase (Fig. 4A, B). In addition, flow cytometric data revealed more cells arrested at the G0/G1 phase and fewer at the S phase at 24 h after drug administration (Fig. 4C). These results confirmed that *Hedyotis diffusae* Herba-*Andrographis* Herba can block the cell cycle, increasing the number of cells arrested at the G0/G1 phase transition and decreasing the number of cells arrested at the S/G2/M phase.

The administration of *Hedyotis diffusae* Herba-*Andrographis* Herba inhibits NPC cell cycle in vivo

In order to further validate the effect of *Hedyotis diffusae* Herba-*Andrographis* Herba on the cell cycle of NPC cells in vivo, we used C666-1 and SUNE-1 cells to construct a mouse xenograft model. FUCCI results showed gradually declined S/G2/M phase-arrested cells and increased G0/G1 phase-arrested cells over time following treatment with *Hedyotis diffusae* Herba-*Andrographis Herba* (Fig. 5A, B). Additionally, flow cytometric analysis revealed more

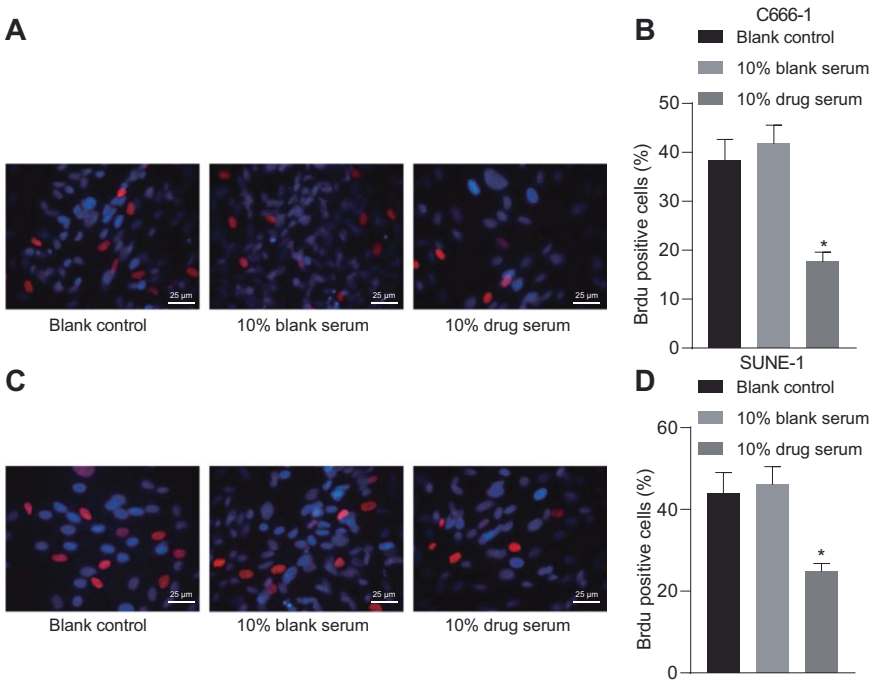

Fig. 1 ***Hedyotis diffusae*** **Herba-*Andrographis* Herba inhibits NPC cell proliferation.** Rat serum was supplemented with *Hedyotis diffusae* Herba-*Andrographis* Herba and added in culture to NPC cells. **A** Representative fluorescence images of Brdu expression in C666-1 cells determined with immunofluorescence staining (scale bar: 25 μm). **B** Quantification of panel **A**. **C** Representative fluorescence images of Brdu expression in SUNE-1 cells determined with immunofluorescence staining (scale bar: 25 μm). **D** Quantification of panel **C**. *$p < 0.05$ vs. the cells treated with blank serum, $n = 3$.

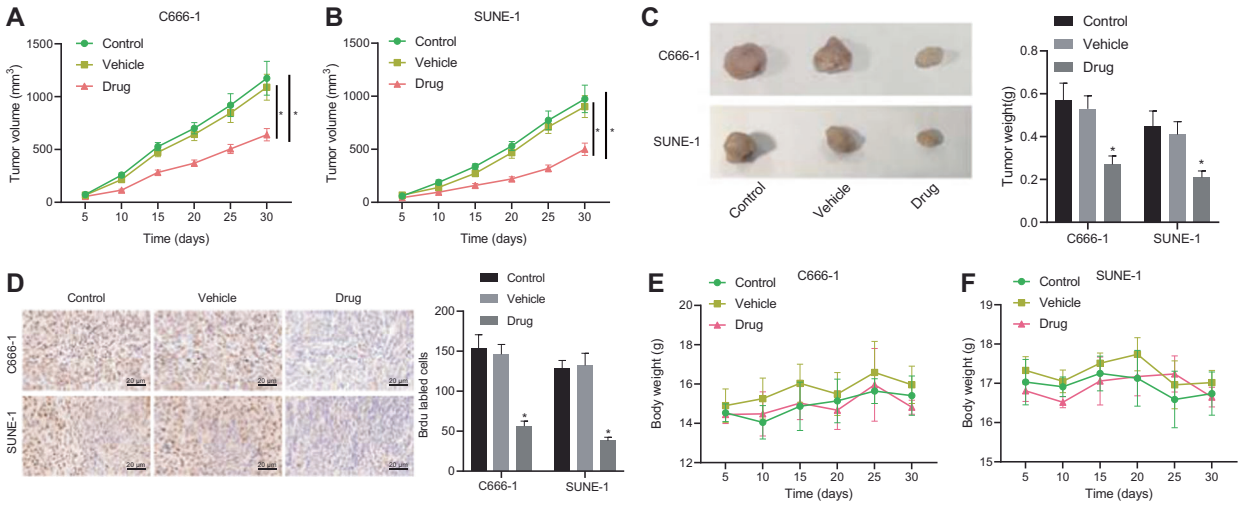

Fig. 2 ***Hedyotis diffusae*** **Herba-*Andrographis* Herba administration suppresses the tumorigenicity of NPC cells in vivo.** **A** Tumor volume of nude mice injected with C666-1 cells. **B** Tumor volume of nude mice injected with SUNE-1 cells. **C** Tumor weight of nude mice injected with C666-1 and SUNE-1 cells. **D** Brdu expression in tumor tissues of nude mice injected with C666-1 and SUNE-1 cells (scale bar = 20 μm). **E** Body weight of C666-1-implanted mice. **F** Body weight of SUNE-1-implanted mice. $n = 6$ for mice in each group. *$p < 0.05$ vs. the mice receiving intragastric administration with normal saline.

C666-1 and SUNE-1 cells arrested at the G0/G1 phase and fewer cells arrested at the S phase at 30 d after the administration of medication compared to baseline (Fig. 5C). This highlights that *Hedyotis diffusae* Herba-*Andrographis* Herba treatment suppresses cell cycle progression from the G1 to S phase in C666-1 and SUNE-1 cells. The administration of *Hedyotis diffusae* Herba-*Andrographis* Herba disrupts cell cycle via the p53/p21/CCND1 axis to inhibit the viability and proliferation of NPC cells.

In order to identify the molecular mechanism by which *Hedyotis diffusae* Herba-*Andrographis* Herba affects NPC, we first analyzed the interaction relationship of 112 candidate genes using the STRING database (Supplementary Table 2) and obtained the interaction relationship network between genes with the Cytoscape 3.5.1 software (Fig. 6A). According to the Degree value of the genes in the network, TP53 (Alias: p53) and STAT3 were at the core of the network. KEGG enrichment analysis indicated that p53 was involved in many signaling pathways, most notably the p53 signaling pathway (hsa04115) (Fig. 6B). The network of p53 and its interaction genes was extracted from Fig. 6A, which indicated that p53 had a close interaction with CDKN1A (Alias:

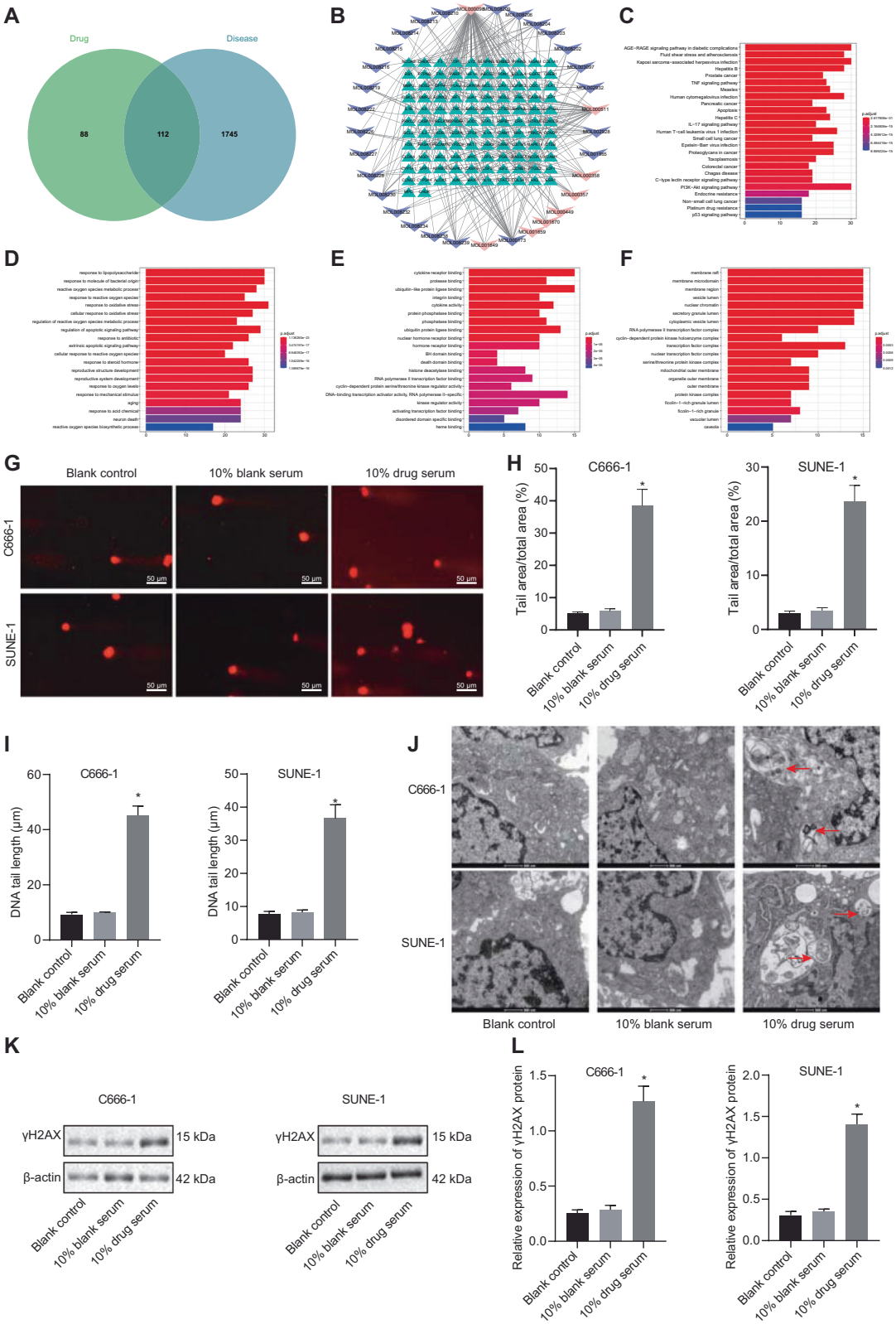

p21) and CCND1 genes (Fig. 6C). Concurrently, previous studies have shown that the regulation on the p53/p21/CCND1 regulatory axis can affect the G1 phase arrest (map04115) [32, 33].

Studies have shown a close correlation of DNA damage with the regulation on the expression of CCND1, p53, and other target proteins. The overexpression of the CCND1 gene can alter cell cycle progression, and the interaction of CCND1 with CDK2 Phospho-Rb and E2F1 contributes to the tumorigenesis [34]. p53 is well-known as a tumor suppressor gene, and p21 is a CDK inhibitor, which plays a tumor-suppressing role together with p53 [28]. Therefore,

Fig. 3 Administration of *Hedyotis diffusae* Herba-*Andrographis* Herba facilitates DNA damage in C666-1 and SUNE-1 cells. A Venn diagram analysis of the predicted targets of *Hedyotis diffusae* Herba-*Andrographis* Herba and therapeutic targets for NPC. **B** Intersection network of candidate targets and the active ingredients of *Hedyotis diffusae* Herba-*Andrographis* Herba. The central green circle represents the candidate gene, and the surrounding polygon represents the molecular ID of the active ingredients, where red color indicates that the ingredient is from *Hedyotis diffusae* Herba, and the purple indicates that the ingredient is from *Andrographis* Herba. **C** KEGG enrichment analysis of candidate genes. **D** BP enrichment analysis of candidate genes. **E** MF enrichment analysis of candidate genes. **F** CC enrichment analysis of candidate genes. **G** Level of DNA damage repair in NPC cells detected by comet assay (red indicates ethidium bromide; scale bar: 50 μm). **H** The percentage of DNA tail area to DNA whole area detected by comet assay. **I** Average comet tail length detected by comet assay. **J** DNA damage of C666-1 and SUNE-1 cells observed under a TEM (scale bar: 1 μm). **K** The protein expression of γH2AX in C666-1 and SUNE-1 cells measured by western blot analysis. **L** Quantification of panel **K**. *$p < 0.05$ vs. the cells treated with blank serum, $n = 3$.

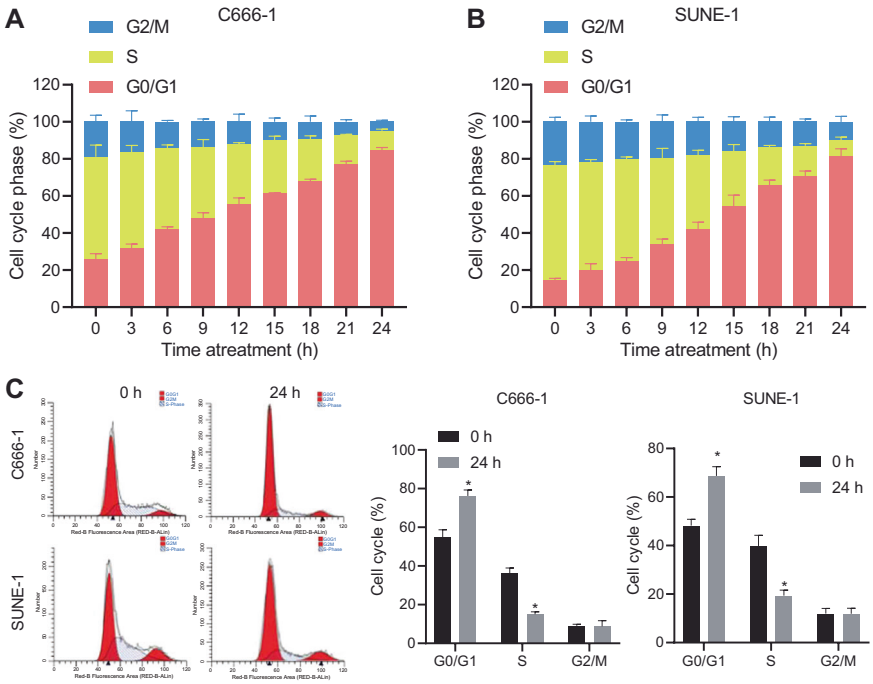

Fig. 4 *Hedyotis diffusae* Herba-*Andrographis* Herba treatment inhibits cell cycle progression in C666-1 and SUNE-1 cells. A C666-1 cell cycle progression was measured by FUCCI. **B** SUNE-1 cell cycle progression measured by FUCCI. **C** Flow cytometric analysis of SUNE-1 and C666-1 cell cycle progression. *$p < 0.05$ vs. the cells treated with *Hedyotis diffusae* Herba-*Andrographis* Herba at 0 h, $n = 3$.

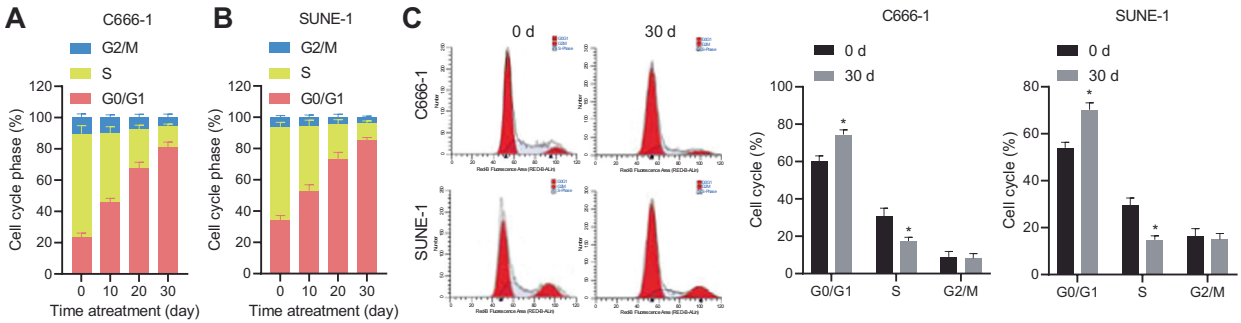

Fig. 5 *Hedyotis diffusae* Herba-*Andrographis* Herba treatment blocks cell cycle progression in vivo. A The C666-1 cell cycle distribution in tumor tissues of C666-1-implanted mice measured by FUCCI. **B** The SUNE-1 cell cycle distribution in tumor tissues of SUNE-1-implanted mice measured by FUCCI. **C** Flow cytometric analysis of SUNE-1 and C666-1 cell cycle distribution in SUNE-1- and C666-1-implanted mice. *$p < 0.05$ vs. the mice treated with *Hedyotis diffusae* Herba-*Andrographis* Herba at 0 h. $n = 6$ for mice in each group.

the detection of CCND1, p53 and related protein expression can reflect the proliferation and apoptosis of NPC cells. Western blot analysis of p53, p21, CCND1, Phospho-Rb, and E2F1 proteins presented no changes in tumor tissues of C666-1- and SUNE-1-implanted mice without treatment or in those treated with normal saline. However, protein expression of p53 and p21 was increased while that of CCND1, Phospho-Rb, and E2F1 was decreased in tumor tissues of C666-1- and SUNE-1-implanted mice treated with medication compared with the normal saline-treated mice (Fig. 6D-F).

PFTα is a p53 inhibitor and UC2288 is a p21 inhibitor [35]. Phospho-Rb and E2F1 are necessary for cell cycle progression from the G1 to S phase [36]. In order to validate whether *Hedyotis diffusae* Herba-*Andrographis* Herba regulates the p53/p21/CCND1

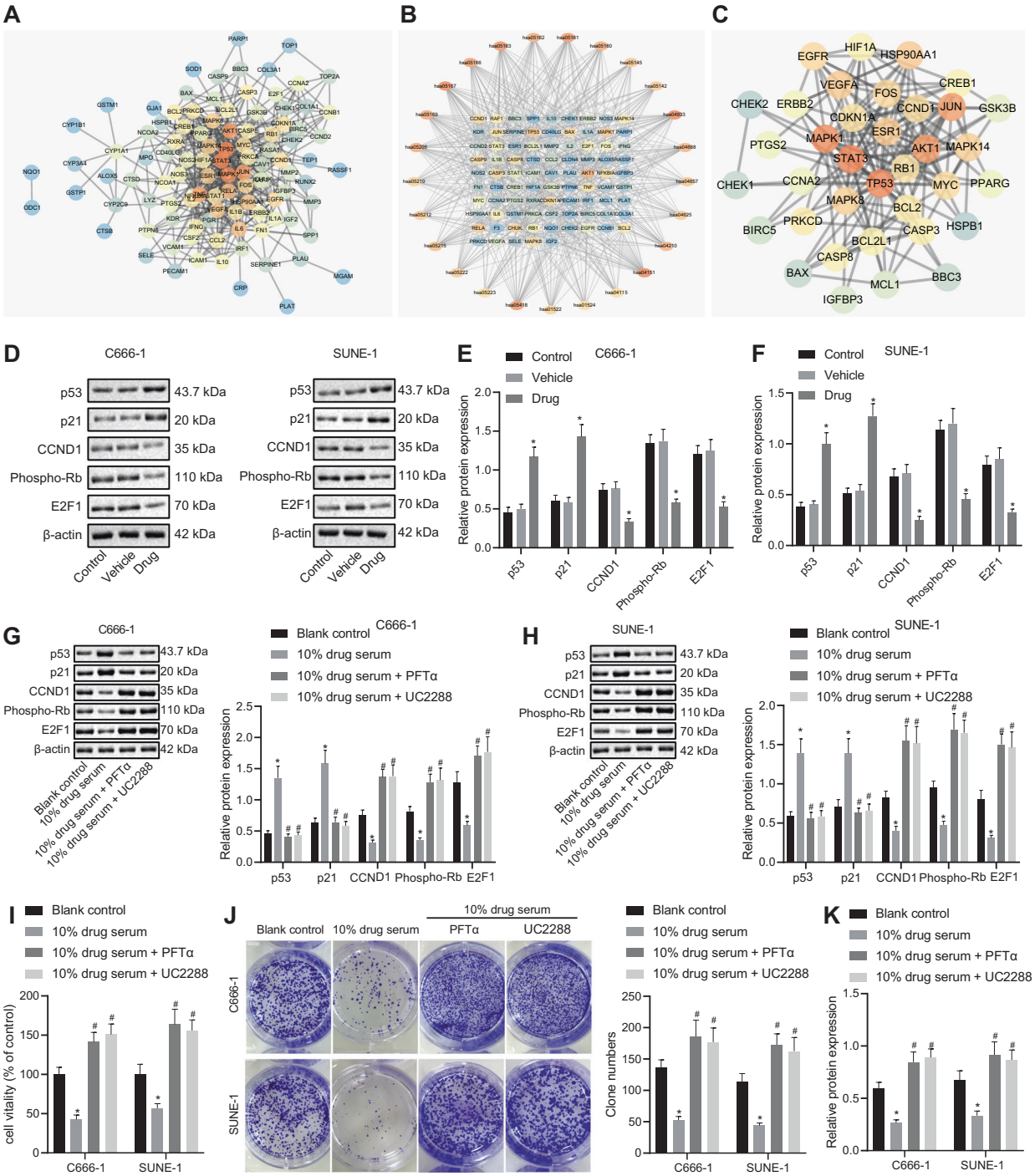

Fig. 6 ***Hedyotis diffusae*** **Herba-*Andrographis* Herba treatment restrains cell cycle progression resulting in decreased viability and proliferation of C666-1 and SUNE-1 cells by altering the p53/p21/CCND1 regulatory axis. A** Interaction relationship network between candidate genes. The color gradation indicated by the circle from blue to orange indicates the Degree value of the gene from small to large. **B** Network diagram of the relationship between the KEGG pathway and genes. **C** Network diagram of TP53 and its interaction genes. **D** Representative western blots of p53, p21, CCND1, Phospho-Rb, and E2F1 proteins in the tumor tissue of C666-1- and SUNE-1-implanted mice. **E** Quantitation of p53, p21, CCND1, Phospho-Rb, and E2F1 protein expression in the tumor tissue of C666-1-implanted mice. **F** Quantitation of p53, p21, CCND1, Phospho-Rb, and E2F1 protein expression in the tumor tissue of SUNE-1-implanted mice. **G** Representative Western blots of p53, p21, CCND1, Phospho-Rb, and E2F1 proteins in C666-1 cells as well as their quantitation. **H** Representative Western blots of p53, p21, CCND1, Phospho-Rb, and E2F1 proteins in SUNE-1 cells as well as their quantitation. **I** Viability of C666-1 and SUNE-1 cells examined using a cell viability test. **J** Proliferation of C666-1 and SUNE-1 cells assessed by colony formation assay. **K** The protein expression of Ki-67 in C666-1 and SUNE-1 cells determined by western blot analysis. $^{*}p < 0.05$ vs. mice receiving intragastric administration with normal saline or the cells without any treatment. $^{\#}p < 0.05$ vs. the cells treated with drug-containing serum. $n = 6$ for mice in each group, $n = 3$.

axis to affect the cell cycle distribution and proliferation of NPC cells, we treated C666-1 and SUNE-1 cells with drug-containing serum + PFTα or drug-containing serum + UC2288. The results of western blot analysis showed that the protein expression of p53 and p21 was significantly augmented while that of CCND1, Phospho-Rb, and E2F1 was reduced in C666-1 and SUNE-1 cells treated with drug-containing serum compared with that in cells without any treatment. Besides, treatment with drug-containing serum + PFTα or drug-containing serum + UC2288 led to lower protein expression of p53 and p21 yet higher protein expression of CCND1, Phospho-Rb, and E2F1 than treatment with drug-containing serum. Additionally, treatment with drug-containing serum suppressed the cell cycle progression of NPC cells from the G1 phase to the S phase, which was revered following treatment with drug-containing serum + PFTα or drug-containing serum + UC2288 (Fig. 6G, H).

The results of cell viability test and colony-formation assay displayed that, in contrast to cells without any treatment, the viability and colony formation of cells treated with drug-containing serum were suppressed. In comparison to cells treated with drug-containing serum, the viability and colony formation of cells treated with drug-containing serum + PFTα or drug-containing serum + UC2288 were increased upon UC2288 treatment (Fig. 6I, J). In addition, Western blot analysis revealed that protein expression of Ki-67 was reduced in cells treated with drug-containing serum, while further PFTα or UC2288 treatment had the opposite effect ($p < 0.05$, Fig. 6K). In summary, *Hedyotis diffusae* Herba-*Andrographis* Herba could regulate the p53/p21/CCND1 axis to suppress cell cycle progression from the G1 to S phase so as to inhibit the viability and proliferation of NPC cells.

DISCUSSION

Natural products can function as antitumor drugs [37]. Traditional Chinese medicine as an adjunct adjunctive therapy has a significant role in raising the life of quality of patients with NPC [38]. This study was designed with the aim to determine the effect of *Hedyotis diffusae* Herba-*Andrographis* Herba on NPC and the molecular mechanism by which these natural treatment ace. Here, we provided evidence, which reveals that these drugs arrest the cell cycle and suppressed cell proliferation of NPC by increasing p53 and p21 expressions through the triggering DNA damage.

The initial finding of our study was that *Hedyotis diffusae* Herba-*Andrographis* Herba could inhibit the proliferation of NPC cells, as demonstrated by reduced tumor volume following drug treatment. Mukonal, another traditional Chinese medicine, has previously been shown to restrain cell proliferation in NPC mouse models [18]. Similarly, the inhibitory role of *Glycyrrhiza glabra* in NPC cell proliferation has been reported by Zheng et al. [39]. One of the recurring themes in the biology and treatment of NPC is the induction of DNA damage. EB virus infection, which can indeed cause DNA damage responses, is usually considered to be the main causative factor in the development of NPC [40]. Our results showed that *Hedyotis diffusae* Herba-*Andrographis* Herba was able to promote DNA damage, accompanied by significantly increased γH2AX expression. Moreover, findings of induced DNA damage accumulation and delayed DNA damage repair were consistent with the promoted sensitivity to irradiation and the chemotherapeutic agent doxorubicin [41]. One of the earliest cellular responses to DNA double-strand breaks is the phosphorylation of γH2AX, meaning that phosphorylated γH2AX can serve as a reliable marker of DNA damage [42]. DNA damage has been documented to be closely related to cell cycle [43]. Interestingly, DNA damage induced by the traditional Chinese medicine Cordycepin has been shown to induce cell cycle arrest [44]. Similarly, our results show that *Hedyotis diffusae* Herba-*Andrographis* Herba treatment blocks NPC cells progression from G1 to S phase, accompanied by elevated expression of p53 and p21 and decreased expression of CCND1, phospho-Rb and E2F1. p53 is a key integrator of cellular responses to DNA damage, contributing to post-translational repair and transcription-mediated responses such as repair and cell cycle arrest [45]. p21 was originally considered to be a cyclin-dependent kinase inhibitor, and a mediator of p53 as well as a sign of cell aging [46]. p21 also closely regulates cell cycle progression and stimulates cell cycle arrest, which can be driven both by p53-dependent or p53-independent mechanisms [47]. The transition of the cells from G1 phase to S phase is a key regulatory checkpoint in controlling the proliferation of eukaryotic cells and the occurrence of tumors [48]. CCND1, also known as Cyclin D1, is a well-known proliferation promoter that accelerates G1/S transition in cell cycle progression [49]. In the context of the cell cycle, Rb is the target of the cyclins-CDK complex, and its phosphorylation is a prerequisite for triggering E2F-dependent gene transcription, which is necessary for cell cycle progression [50]. Interestingly, a previous study has suggested that *Andrographolide* could enhance G1 phase block, decrease the protein expression of CCND1 and CDK4, and increase expression of p53 and p21, as well as suppressing phosphorylation of Rb and dissociation of the Rb/E2F complex [51]. Besides, downregulated expression of CDK4/6, CCND1, E2F1 and upregulated the expression of p21 can restrain the cell cycle progression of NCP cells [52]. In addition, G1 phase arrest induced by Luteolin presented with inhibited cyclin D1 expression, CDK4/6 activity, Rb phosphorylation, as well as E2F1 expression in NPC [53]. All these results are conducive with the findings made in this study. Furthermore, the present findings supports the hypothesis that activation of p53 results in elevated expression of p21 and diminished expression of CCND1, Phospho-Rb, E2F1, whereas inhibition of p21 led to increased expression of CCND1, Phospho-Rb, and E2F1.

In conclusion, the current study reveals that *Hedyotis diffusae* Herba-*Andrographis* Herba inhibit cell cycle progression from G1 phase to S phase and thereby impede the proliferation of NPC

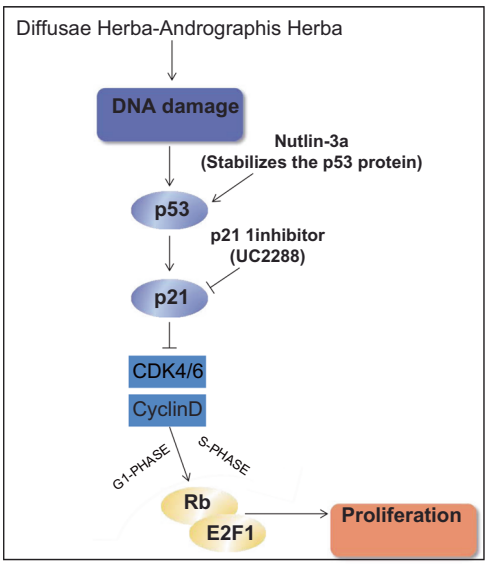

Fig. 7 Schematic diagram summarizing the effects of *Hedyotis diffusae* Herba-*Andrographis* Herba on cell cycle progression and proliferation of NPC. Administration of *Hedyotis diffusae* Herba-*Andrographis* Herba regulates the p53/p21/CCND1 axis to induce DNA damage and block cell cycle progression from the G1 phase to the S phase, thereby inhibiting the viability and proliferation of NPC cells.

cells via inhibition of the CCND1/Rb/E2F1regulatory axis through DNA damage-induced activation of p53 and p21 (summarized in Fig. 7). This improves our r understanding of NPC progression and highlights a novel potential therapeutic treatment for NPC. This study, for the first time combined the components of *Hedyotis diffusae* Herba-*Andrographis* Herba and conducted an in-depth investigation of the mechanism of this mixture in the treatment of NPC, providing a reliable basis for explaining its molecular mechanism in the treatment of NPC. Nevertheless, the current study presents the theoretical basis of this mechanism in NPC, and calls for detailed investigation of effects of CCND1, Phospho-Rb, E2F1 on the development of NPC cells. In addition, the optimal composition and dosage of *Hedyotis diffusae* Herba-*Andrographis* Herba remains to be established in future work.

REFERENCES

1. Le QT, Colevas AD, O'Sullivan B, Lee AWM, Lee N, Ma B, et al. Current treatment landscape of nasopharyngeal carcinoma and potential trials evaluating the value of immunotherapy. J Natl Cancer Inst. 2019;111:655–63.
2. Chen YP, Chan ATC, Le QT, Blanchard P, Sun Y, Ma J. Nasopharyngeal carcinoma. Lancet. 2019;394:64–80.
3. Bruce JP, Yip K, Bratman SV, Ito E, Liu FF. Nasopharyngeal cancer: molecular landscape. J Clin Oncol. 2015;33:3346–55.
4. Nor Hashim NA, Ramzi NH, Velapasamy S, Alex L, Chahil JK, Lye SH, et al. Identification of genetic and non-genetic risk factors for nasopharyngeal carcinoma in a Southeast Asian population. Asian Pac J Cancer Prev. 2012;13:6005–10.
5. Chua MLK, Wee JTS, Hui EP, Chan ATC. Nasopharyngeal carcinoma. Lancet. 2016;387:1012–24.
6. Wei KR, Zheng RS, Zhang SW, Liang ZH, Li ZM, Chen WQ. Nasopharyngeal carcinoma incidence and mortality in China, 2013. Chin J Cancer. 2017;36:90.
7. So TH, Chan SK, Lee VH, Chen BZ, Kong FM, Lao LX. Chinese medicine in cancer treatment—how is it practised in the east and the west? Clin Oncol (R Coll Radiol). 2019;31:578–88.
8. Carmady B, Smith CA. Use of Chinese medicine by cancer patients: a review of surveys. Chin Med. 2011;6:22.
9. Liao YH, Lin CC, Lai HC, Chiang JH, Lin JG, Li TC. Adjunctive traditional Chinese medicine therapy improves survival of liver cancer patients. Liver Int. 2015;35:2595–602.
10. Lee YW, Chen TL, Shih YR, Tsai CL, Chang CC, Liang HH, et al. Adjunctive traditional Chinese medicine therapy improves survival in patients with advanced breast cancer: a population-based study. Cancer. 2014;120:1338–44.
11. Zhu D, Shao M, Yang J, Fang M, Liu S, Lou D, et al. Curcumin enhances radiosensitization of nasopharyngeal carcinoma via mediating regulation of tumor stem-like cells by a CircRNA network. J Cancer. 2020;11:2360–70.
12. Song YC, Hung KF, Liang KL, Chiang JH, Huang HC, Lee HJ, et al. Adjunctive Chinese herbal medicine therapy for nasopharyngeal carcinoma: clinical evidence and experimental validation. Head Neck. 2019;41:2860–72.
13. HU LWH, CUI N. Effect of herba Hedyotis diffusa on living murine ascites hepatoma H22 cells and T lymphocytes[J]. J Guangzhou Univ Traditional Chin Med. 2007;24:313–6.
14. Wang CY, Wang TC, Liang WM, Hung CH, Chiou JS, Chen CJ, et al. Effect of Chinese Herbal Medicine therapy on overall and cancer related mortality in patients with advanced nasopharyngeal carcinoma in Taiwan. Front Pharmacol. 2020;11:607413.
15. Lim JC, Chan TK, Ng DS, Sagineedu SR, Stanslas J, Wong WS. Andrographolide and its analogues: versatile bioactive molecules for combating inflammation and cancer. Clin Exp Pharmacol Physiol. 2012;39:300–10.
16. Wu B, Chen X, Zhou Y, Hu P, Wu D, Zheng G, et al. Andrographolide inhibits proliferation and induces apoptosis of nasopharyngeal carcinoma cell line C666-1 through LKB1-AMPK-dependent signaling pathways. Pharmazie. 2018;73:594–7.
17. Su EY, Chu YL, Chueh FS, Ma YS, Peng SF, Huang WW, et al. Bufalin induces apoptotic cell death in human nasopharyngeal carcinoma cells through mitochondrial ROS and TRAIL pathways. Am J Chin Med. 2019;47:237–57.
18. Guo Y, Hao Y, Guan G, Ma S, Zhu Z, Guo F, et al. Mukonal inhibits cell proliferation, alters mitochondrial membrane potential and induces apoptosis and autophagy in human CNE1 nasopharyngeal carcinoma cells. Med Sci Monit. 2019;25:1976–83.
19. Pan Z, Luo Y, Xia Y, Zhang X, Qin Y, Liu W, et al. Cinobufagin induces cell cycle arrest at the S phase and promotes apoptosis in nasopharyngeal carcinoma cells. Biomed Pharmacother. 2020;122:109763.
20. Rajagopal S, Kumar RA, Deevi DS, Satyanarayana C, Rajagopalan R. Andrographolide, a potential cancer therapeutic agent isolated from Andrographis paniculata. J Exp Ther Oncol. 2003;3:147–58.
21. Khole S, Mittal S, Jagadish N, Ghosh D, Gadgil V, Sinkar V, et al. Andrographolide enhances redox status of liver cells by regulating microRNA expression. Free Radic Biol Med. 2019;130:397–407.
22. Fischer M, Quaas M, Steiner L, Engeland K. The p53-p21-DREAM-CDE/CHR pathway regulates G2/M cell cycle genes. Nucleic Acids Res. 2016;44:164–74.
23. Wang Z, Mao JW, Liu GY, Wang FG, Ju ZS, Zhou D, et al. MicroRNA-372 enhances radiosensitivity while inhibiting cell invasion and metastasis in nasopharyngeal carcinoma through activating the PBK-dependent p53 signaling pathway. Cancer Med. 2019;8:712–28.
24. Weng C, Chen Y, Wu Y, Liu X, Mao H, Fang X, et al. Silencing UBE4B induces nasopharyngeal carcinoma apoptosis through the activation of caspase3 and p53. Onco Targets Ther. 2019;12:2553–61.
25. Zlotorynski E. Tumour suppressors: the dark side of p21. Nat Rev Cancer. 2016;16:481.
26. Jiang X, Liu W. Long noncoding RNA highly upregulated in liver cancer activates p53-p21 pathway and promotes nasopharyngeal carcinoma cell growth. DNA Cell Biol. 2017;36:596–602.
27. Zhang Y, Miao Y, Shang M, Liu M, Liu R, Pan E, et al. LincRNA-p21 leads to G1 arrest by p53 pathway in esophageal squamous cell carcinoma. Cancer Manag Res. 2019;11:6201–14.
28. Vilgelm AE, Saleh N, Shattuck-Brandt R, Riemenschneider K, Slesur L, Chen SC, et al. MDM2 antagonists overcome intrinsic resistance to CDK4/6 inhibition by inducing p21. Sci Transl Med. 2019;11:505.
29. Li Y, Li Y, Zou Z, Li Y, Xie H, Yang H. Yin Yang Gong Ji pill is an ancient formula with antitumor activity against hepatoma cells. J Ethnopharmacol. 2020;248:112267.
30. Vodenkova S, Azqueta A, Collins A, Dusinska M, Gaivao I, Moller P, et al. An optimized comet-based in vitro DNA repair assay to assess base and nucleotide excision repair activity. Nat Protoc. 2020;15:3844–78.
31. Bouchard G, Therriault H, Geha S, Berube-Lauziere Y, Bujold R, Saucier C, et al. Stimulation of triple negative breast cancer cell migration and metastases formation is prevented by chloroquine in a pre-irradiated mouse model. BMC Cancer. 2016;16:361.
32. Huang H, Han Y, Yang X, Li M, Zhu R, Hu J, et al. HNRNPK inhibits gastric cancer cell proliferation through p53/p21/CCND1 pathway. Oncotarget. 2017;8:103364–74.
33. Guo Q, Yin X, Gao J, Wang X, Zhang S, Zhou X, et al. MiR-381-3p redistributes between cytosol and mitochondria and aggravates endothelial cell injury induced by reactive oxygen species. Tissue Cell. 2020;67:101451.
34. Chen S, Luo T, Yu Q, Dong W, Zhang H, Zou H. Isoorientin plays an important role in alleviating Cadmium-induced DNA damage and G0/G1 cell cycle arrest. Ecotoxicol Environ Saf. 2020;187:109851.
35. Gupta R, Dong Y, Solomon PD, Wettersten HI, Cheng CJ, Min JN, et al. Synergistic tumor suppression by combined inhibition of telomerase and CDKN1A. Proc Natl Acad Sci USA. 2014;111:E3062–71.
36. Reuther C, Heinzle V, Nolting S, Herterich S, Hahner S, Halilovic E, et al. The HDM2 (MDM2) inhibitor NVP-CGM097 inhibits tumor cell proliferation and shows additive effects with 5-fluorouracil on the p53-p21-Rb-E2F1 cascade in the p53 wild type neuroendocrine tumor cell line GOT1. Neuroendocrinology. 2018;106:1–19.
37. Newman DJ, Cragg GM. Natural products as sources of new drugs from 1981 to 2014. J Nat Prod. 2016;79:629–61.
38. Mao CG, Tao ZZ, Wan LJ, Han JB, Chen Z, Xiao BK. The efficacy of traditional Chinese Medicine as an adjunctive therapy in nasopharyngeal carcinoma: a systematic review and meta-analysis. J BUON. 2014;19:540–8.
39. Zheng C, Han L, Wu S. A metabolic investigation of anticancer effect of G. glabra root extract on nasopharyngeal carcinoma cell line, C666-1. Mol Biol Rep. 2019;46:3857–64.
40. Poon RY. DNA damage checkpoints in nasopharyngeal carcinoma. Oral Oncol. 2014;50:339–44.
41. Ma J, Sun F, Li C, Zhang Y, Xiao W, Li Z, et al. Depletion of intermediate filament protein Nestin, a target of microRNA-940, suppresses tumorigenesis by inducing spontaneous DNA damage accumulation in human nasopharyngeal carcinoma. Cell Death Dis. 2014;5:e1377.
42. Siddiqui MS, Francois M, Fenech MF, Leifert WR. Persistent gammaH2AX: a promising molecular marker of DNA damage and aging. Mutat Res Rev Mutat Res. 2015;766:1–19.
43. Dhuppar S, Mazumder A. Measuring cell cycle-dependent DNA damage responses and p53 regulation on a cell-by-cell basis from image analysis. Cell Cycle. 2018;17:1358–71.
44. Liao Y, Ling J, Zhang G, Liu F, Tao S, Han Z, et al. Cordycepin induces cell cycle arrest and apoptosis by inducing DNA damage and up-regulation of p53 in Leukemia cells. Cell Cycle. 2015;14:761–71.
45. Sun B, Ross SM, Rowley S, Adeleye Y, Clewell RA. Contribution of ATM and ATR kinase pathways to p53-mediated response in etoposide and methyl methanesulfonate induced DNA damage. Environ Mol Mutagen. 2017;58:72–83.

46. Jung YS, Qian Y, Chen X. Examination of the expanding pathways for the regulation of p21 expression and activity. Cell Signal. 2010;22:1003–12.
47. Karimian A, Ahmadi Y, Yousefi B. Multiple functions of p21 in cell cycle, apoptosis and transcriptional regulation after DNA damage. DNA Repair (Amst). 2016;42:63–71.
48. Bertoli C, Skotheim JM, de Bruin RA. Control of cell cycle transcription during G1 and S phases. Nat Rev Mol Cell Biol. 2013;14:518–28.
49. Stacey DW. Cyclin D1 serves as a cell cycle regulatory switch in actively proliferating cells. Curr Opin Cell Biol. 2003;15:158–63.
50. Bendris N, Lemmers B, Blanchard JM. Cell cycle, cytoskeleton dynamics and beyond: the many functions of cyclins and CDK inhibitors. Cell Cycle. 2015;14:1786–98.
51. Shi MD, Lin HH, Lee YC, Chao JK, Lin RA, Chen JH. Inhibition of cell-cycle progression in human colorectal carcinoma Lovo cells by andrographolide. Chem Biol Interact. 2008;174:201–10.
52. Liu Z, Long X, Chao C, Yan C, Wu Q, Hua S, et al. Knocking down CDK4 mediates the elevation of let-7c suppressing cell growth in nasopharyngeal carcinoma. BMC Cancer. 2014;14:274.
53. Ong CS, Zhou J, Ong CN, Shen HM. Luteolin induces G1 arrest in human nasopharyngeal carcinoma cells via the Akt-GSK-3beta-Cyclin D1 pathway. Cancer Lett. 2010;298:167–75.

AUTHOR CONTRIBUTIONS

ZL and SM conceived and designed research. SL and JL performed experiments. YD and ZY interpreted results of experiments. JL and LC analyzed data. QF and XC prepared figures. LD and RH drafted paper. QZ and HX edited and revised manuscript. All authors read and approved final version of manuscript.

FUNDING

This study was supported by the National Twelfth Five-Year Support Plan (No. 2015BAI04B00), and National Natural Science Foundation of China (No. 81273985 & 81403440).

COMPETING INTERESTS

The authors declare no competing interests.

ETHICS APPROVAL

The experiments involving animals were performed under approval of the Institutional Animal Care and Use Committee of the Affiliated Hospital of Chengdu University of Traditional Chinese Medicine and in compliance with the recommendations in the Guide for the Care and Use of Laboratory Animals published by the US National Institutes of Health. All efforts were made to minimize the number and suffering of the animals.

ADDITIONAL INFORMATION

Supplementary information The online version contains supplementary material available at https://doi.org/10.1038/s41417-021-00385-7.

Correspondence and requests for materials should be addressed to Qinxiu Zhang or Hui Xie.